fluids

MDPI

Article

Numerical Modeling of the Wave-Plate-Current Interaction by the Boundary Element Method

Hasna Akarni *, Laila El Aarabi, Laila Mouakkir and Soumia Mordane

Laboratory of Polymer Physics, Mechanical Sciences and Materials, Faculty of Sciences Ben M'sik Sidi Othman, University Hassan II, P.B 7955 Sidi Othman, Casablanca 20670, Morocco; laila.elaarabi@gmail.com (L.E.A.); mouakkir.leila@gmail.com (L.M.); soumia.mordane@etu.univh2c.ma (S.M.)

* Correspondence: hasnaakarni97@gmail.com

Abstract: The aim of this work is to propose a numerical study of the interaction of a wave-horizontal plate fixed and completely immersed in a flat-bottomed tank with a uniform current flowing in the same direction as the incident wave. We investigate in particular the effect of the plate at minimizing the impact of the wave on the coast of beaches by studying the free surface elevation and the reflection coefficient, as well as the influence of the various geometrical parameters on the latter, taking into account the presence of the current. The numerical method used in this study is the boundary element method (BEM), and the results obtained will be confronted with experimental and analytical data existing in the literature.

Keywords: wave; current; plate; boundary element method (BEM); numerical wave tank (NWT); reflection coefficient; free surface elevation

Citation: Akarni, H.; El Aarabi, L.; Mouakkir, L.; Mordane, S. Numerical Modeling of the Wave-Plate-Current Interaction by the Boundary Element Method. *Fluids* **2021**, *6*, 435. https://doi.org/10.3390/fluids6120435

Academic Editor: Sheldon Wang

Received: 7 November 2021
Accepted: 25 November 2021
Published: 1 December 2021

1. Introduction

The ocean surface is disturbed by numerous physical phenomena that cause deformation of the free surface and lead to a transfer of mechanical energy that manifests itself in the formation and propagation of an indefinite suite of nearly identical parallel ripples. The latter propagate fairly uniformly from the open ocean to the coast, known as a wave. These events and their impact on our continent arouse the interest of many researchers who have devoted much effort to understanding and modeling the wave.

Numerous experimental, analytical and numerical studies have treated the wave-obstacle interaction with and without current. Brossard and Chagdali in 2001 [1] studied the problem of wave-plate interaction experimentally by using a moving probe, which allowed measuring the reflection and transmission coefficients of a horizontal plate immersed at different depths. In 2009, Brossard et al. [2] improved their research by adding the Doppler method to quantify the process of wave decomposition over a submerged structure (plate or step). Liu et al. [3] numerically studied the problem presented by Brossard [2] using the desingularized boundary integral equation method (DBIEM). Xie, Z. et al. in 2020 [4] presented a numerical study of multiphase flow for performing large-eddy simulations of various three-dimensional wave-structure interaction problems featuring complex geometries, such as a 3D traveling wave in a closed channel, a 3D solitary wave interacting with a vertical circular cylinder, a 3D solitary wave interacting with a thin horizontal plate, and a 3D focusing wave impacting on an FPSO-like structure. In 2020, El Aarabi et al. [5] numerically studied the problem of wave interaction with two rectangular obstacles spaced and fixed on the bottom of the numerical wave tank (NWT) using the boundary element method (BEM).

The propagation of the wave is generally accompanied by currents, and thus many researchers have worked on this problem. Zou et al. in 2013 [6] developed a new formulation for the Boussinesq-type equations by using a perturbation method to explicitly reveal the effect of the current on the vertical distributions of the wave velocity and the pressure. In

2014, Ning et al. [7] presented a numerical study of the higher harmonics in the interaction of a nonlinear wave with a horizontal cylinder in the presence of a uniform current. In 2017, Bai et al. [8] studied the interaction between the wave, current and a horizontal cylinder located near the free surface experimentally and numerically by determining the forces exerted on the horizontal cylinder. In 2016, Lim et al. [9] made an experimental study on a near-orthogonal wave-current interaction over smooth and uniform fixed roughness beds; this study also aimed at understanding the changes in wave-induced mass transport flows due to wave-current interactions. In 2018, Fan et al. [10] combined the finite difference method with the Runge-Kutta method to investigate the wave-current interaction in flumes with horizontal and inclined bottoms. In 2019, Yu Hsiao et al. [11] presented a numerical simulation of wave-current interaction with a sinusoidal bottom using an open-source computational fluid dynamics software package (OpenFOAM).

As in our work, several researchers have analyzed the effect of current on the wave-plate interaction. In 2002, Rey et al. [12] experimentally studied the influence of a homogeneous current in the same direction of the incident wave on the reflection coefficient produced due to a submerged plate. The same author in 2011 [13] extended his experimental study by treating the problem of wave-plate interaction in the presence of the current for regular and irregular waves. Zhang et al. in 2020 [14] presented experiments and numerical simulations to investigate the wave-current forces on coastal bridge superstructures with box girders. The aim of this study was to enhance the understanding of the mechanism of bridge damage by waves and currents. In 2019, Ning et al. [15] used the potential theory to estimate the forces and moment on a submerged plate induced by the wave-current interaction. In 2016, Errifaiy et al. [16] conducted an analytical study of the wave-plate-current interaction, and the study was based on the potential theory linearized with the model of evanescent modes. Thus, they introduced in 2019 the influence of geometric parameters on the reflection coefficient [17]. In this present work, the wave-plate-current interaction is explored using the boundary element method (BEM). To validate the proposed approach, a comparison between the obtained results, those of the experiment and the analytical ones are presented. A study of the influence of the current on the free surface elevation and the reflection coefficient, as well as the effect of the geometrical parameters on the latter, is revealed.

2. Materials and Methods

We consider a geometrical domain D, where a monochromatic incident wave of low amplitude is propagating in the same direction as a uniform current of a horizontal velocity U. In the presence of a plate of length l and thickness e is fixed in a tank with a flat bottom of length L and depth H. The plate is immersed at a depth h below the position taken by the free surface at rest. As seen in Figure 1, Γ_U stands for the upstream boundary, Γ_F the free surface boundary, Γ_B the object and bottom boundaries and Γ_D the downstream boundary.

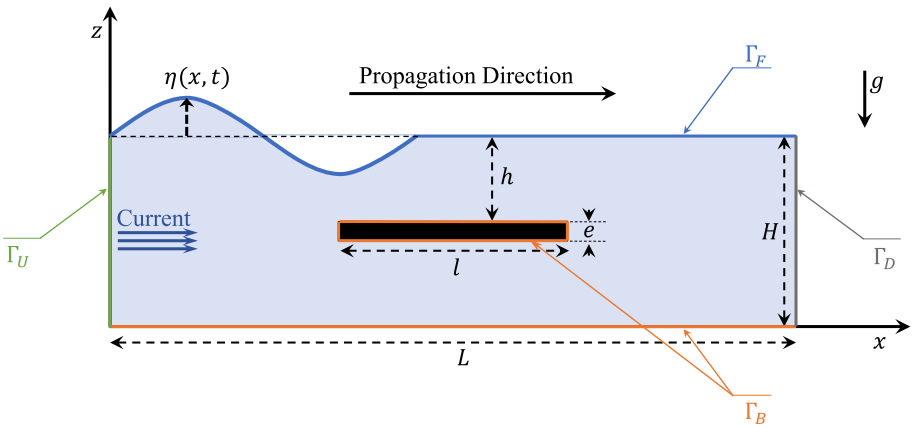

Figure 1. Descriptive schemas of the problem studied.

It is assumed that the fluid is perfect and incompressible, and the flow is considered two-dimensional and irrotational. Under these assumptions, the two-dimensional problem of a linear wave is reduced to determining the velocity potential $\Phi(x,z,t)$ and the free surface elevation $\eta(x,t)$. These two variables will be assumed to be complex with harmonic dependence on time. The velocity potential $\Phi(x,z,t)$ can be represented as follows:

$$\Phi(x,z,t) = \Phi_c(x) + \Phi_w(x,z,t) \tag{1}$$

where $\Phi_c(x) = U \cdot x$ is the velocity potential associated to the current and $\Phi_w(x,z,t) = \phi_w(x,z)exp(i\omega t)$ refers to the velocity potential associated to the wave. U, i and t are respectively the velocity of the current, the complex number and the temporal variable. The above equation is completed by the boundary conditions as follows:

$$\begin{cases} \Delta\phi_w = 0 & \text{in } D \\ \dfrac{\partial\phi_w}{\partial n} = -ik^-\phi_w + i(k^- + k^+)f(z) & \text{on } \Gamma_U \\ \dfrac{\partial\phi_w}{\partial n} = 0 & \text{on } \Gamma_B \\ \dfrac{\partial\phi_w}{\partial n} = \dfrac{\omega c_0^2(2Uk-\omega)}{g(U^2-c_0^2)}\phi_w & \text{on } \Gamma_F \\ \dfrac{\partial\phi_w}{\partial n} = -ik^+\phi_w & \text{on } \Gamma_D \\ \eta = -\dfrac{i(\omega - k^+U)}{g}\Phi_w - \dfrac{U^2}{2g} & \text{the free surface elevation} \end{cases} \tag{2}$$

where n is the exterior normal on the entire computational boundary ($\partial D = \Gamma_U \cup \Gamma_B \cup \Gamma_D \cup \Gamma_F$), which bounds the global domain (D), g is the gravitational acceleration, k is the wavenumber of the incident wave in the absence of the current, k^+ and k^- are, respectively, the wavenumber of the incident and reflected wave in the presence of the current, $\omega = \dfrac{2\pi}{T}$ is the angular frequency (T is the wave period of incident wave) and c_0 is the incident wave's celerity in the absence of current, equal to:

$$c_0 = \sqrt{\frac{gk \cdot tanh(kH)}{kH}} \tag{3}$$

where $f(z)$ is a function that is related to the wave's characteristics, such that:

$$f(z) = \frac{a_i g}{(\omega - k^+U)\, cosh(k^+H)}\, cosh(k^+z) \tag{4}$$

Note that a_i is the amplitude of the incident wave in the presence of the current, and the constants k^- end $k^+$are the solutions of the dispersion equations. Generally, the dispersion relation in the presence of a uniform current U is defined by:

$$(\omega \mp Uk^\pm)^2 = gk^\pm tanh(k^\pm H) \tag{5}$$

We note that the set of boundary conditions for Equation (2) is expressed as relations between the potential ϕ_w and its normal derivative $\dfrac{\partial\phi_w}{\partial n}$. This justifies the choice of the boundary element method.

3. Numerical Formulation

Many branches of physics and mechanics use the boundary element method [18]. It is mostly used to solve problems governed by linear partial differential equations numerically. The discretization of the BEM is limited to the interfaces of different environments, which is perhaps its most important feature. The boundary element method is applied in many fields of physics and mechanics. It mainly allows the numerical solution of problems

governed by linear partial differential equations. Perhaps the most important feature of the BEM is that the discretisation is only on the interfaces of the different media. This feature reduces the size of the problem and makes the meshing simpler and faster.

This property minimizes the problem's dimension, which makes meshing easier and faster.

Applying Green's second identity, we can express ϕ_w in integral form as follows:

$$c\phi_w(x,z) = \int_{\partial D}\left[\frac{\partial \phi_w(x',z')}{\partial n}G(r) - \frac{\partial G(r)}{\partial n}\phi_w(x',z')\right]ds \tag{6}$$

where $c = 0$ if the coordinate points $(x,z) \notin D \cup \partial D$, $c = 0.5$ if the coordinate points $(x,z) \in \partial D$ and $c = 1$ if the coordinate points $(x,z) \in D$. $G(r) = -\frac{1}{2\pi}ln(r)$ is the Green's function with $r = \sqrt{(x-x')^2 + (z-z')^2}$ is the distance between a field point and a boundary point.

In the numerical formulation, the boundaries are subdivided into a finite number of N segments. We subdivide the bottom boundary into N_1 elements, the downstream boundary in N_2 elements, the free surface in N_3 elements, the upstream boundary in N_4 elements, the upper border of the plate in N_5 elements, the right border of the plate in N_6 elements, the lower border of the plate in N_7 elements and the left border of the plate in N_8 elements. Therefore, N will be $N = \sum_{i=1}^{8} N_i$ Figure 2.

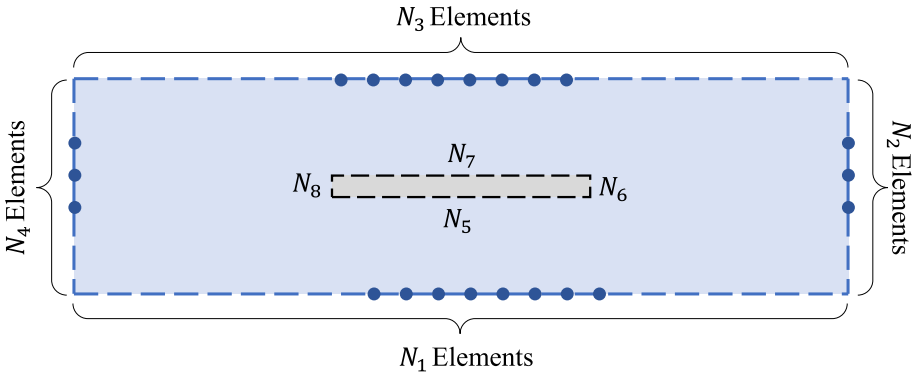

Figure 2. Descriptive schematic of the mesh.

To numerically obtain the velocity potential ϕ_w and its normal derivative $\frac{\partial \phi_w}{\partial n}$ on the set of domain boundaries, those latter are subdivided into small segments of length Δs and a singularity is imposed on each segment. The integral of each segment can be obtained in different ways. For example, by imposing a localized singularity in the middle of each segment, computing the potential ϕ_w on the boundaries reduces to solving a matrix system.

$$c\phi_w^i = \sum_{j=1}^{N} E_{ij}\frac{\partial \phi_w^j}{\partial n_j} - H_{ij}\phi_w^j \tag{7}$$

The explicit form of the influence matrices H and E is as follows:

- For $i \neq j$: $H_{ij} = \int_{\Delta s_j}\frac{\partial G}{\partial n}ds = \frac{\partial}{\partial n}(ln(\frac{1}{r}))\Delta s_j$ and $E_{ij} = \int_{\Delta s_j} Gds = ln(\frac{1}{r})\Delta s_j$
- For $i = j$: $H_{ij} = 2\pi$ and $E_{ij} = 2(1 - log(\Delta s_j))\Delta s_j$

We can then transform Equation (7) into a relation between the unknown ϕ_w and its normal derivative $\frac{\partial \phi_w}{\partial n}$ on the contour ∂D. The new matrix form of the relation in Equation (7) is written as:

$$\{\phi_w\} = [K]\left\{\frac{\partial \phi_w}{\partial n}\right\} \tag{8}$$

This system consists of N equations with $2N$ unknowns, which are the potential and its normal derivative on the study domain's boundaries, respectively. The N additional equations are obtained by writing the boundary conditions. These boundary conditions can be expressed by relations between the two unknowns of the form:

$$\left\{\frac{\partial \phi_w}{\partial n}\right\} = [F]\{\phi_w\} + \{SN\} \tag{9}$$

By inserting Equation (9) into (8), the determination of the velocity potential associated with the wave ϕ_w thus reduces to solving the following system:

$$[L]\{\phi_w\} = \{SN\} \tag{10}$$

where $[L] = \left([K]^{-1} - [F]\right)$ is the tangent matrix, and $\{SN\}$ is the right-hand side vector.

With regard to the application of the numerical method, we found that there exists a correlation between the wavelength λ and the boundary discretization step Δs. From the numerical tests, we found that it is necessary to respect the following inequality:

$$\frac{\Delta s}{\lambda} < \frac{1}{9} \tag{11}$$

This result, Equation (11), is also mentioned by other authors [19,20].

4. Results and Discussions

4.1. Validation of the Numerical Code: (Absence of the Current)

4.1.1. Case of Flat-Bottom

In this part, we will validate the proposed numerical approach by comparing its results with the experimental and analytical ones. We begin by studying the propagation of the wave, which lies in the free surface elevation, in the presence of a flat bottom (Figure 3). For this, we consider a monochromatic incident wave, which has an amplitude $a = 0.01$ m and wavelength $\lambda = 9$ m, and propagates in a numerical wave tank (NWT) of length $L = 30$ m and depth $H = 2.5$ m.

Figure 3a presents the numerical free surface elevation along the tank during different time instants (from 0 to T with the time increment $\Delta t = \frac{T}{10}$). On the other hand, Figure 3b depicts the effect of the mesh on the convergence of the numerical solution obtained by the BEM with the analytical solution of stokes at order 1 [21] for a period. From this figure, we can see that the more refined the mesh is, the more the solution converges to the analytical solution, which allows validating the numerical approach used.

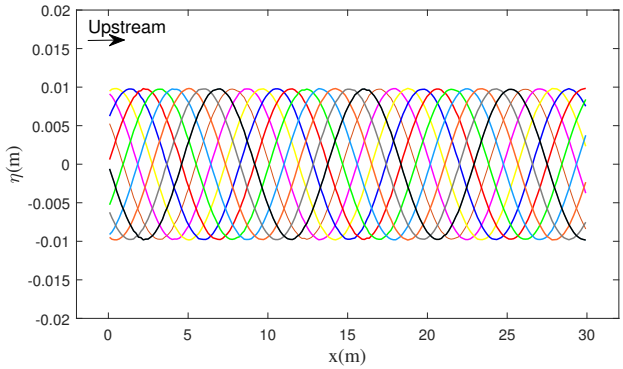

(**a**)

Figure 3. *Cont.*

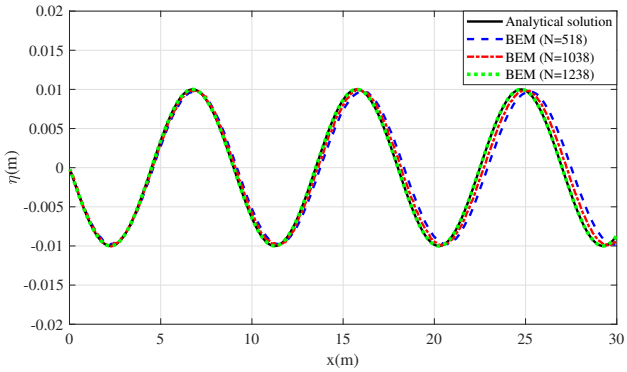

(**b**)

Figure 3. Elevation of the numerical free surface as a function of channel length. (**a**): For different instants of time. (**b**): For $t = T$.

4.1.2. Case of Wave-Submerged Plate Interaction

Another comparison to affirm the effectiveness of the numerical approach used concerns the reflection coefficient R. This comparison is based on experimental measurements established by Brossard and Chagdali [1], who took a plate of thickness $e = 0.002$ m, length $l = 25$ cm and a water depth $H = 0.188$ m for different values of relative immersion $(h/H = 0.24, 0.48, 0.74)$. Figure 4 shows the variation of the reflection coefficient R as a function of the incident wavenumber k. These curves demonstrate that there is a good agreement between the results calculated by the BEM and those measured experimentally.

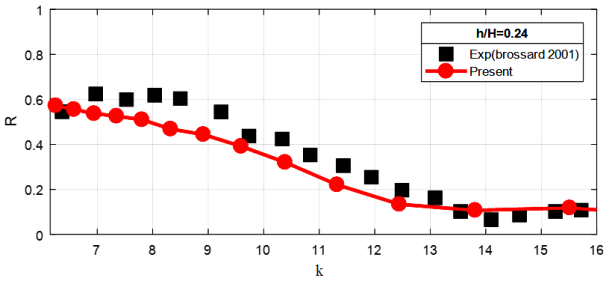

(**a**)

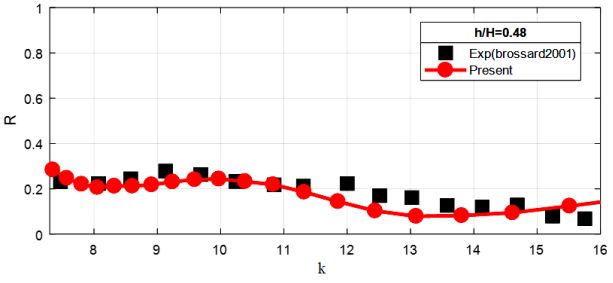

(**b**)

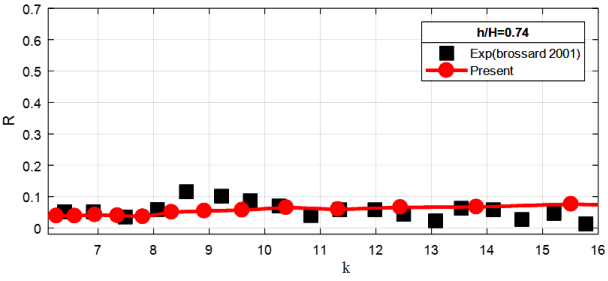

(**c**)

Figure 4. Reflection coefficient R as a function of k for different values of relative immersion of the plate (**a**): $h/H = 0.24$. (**b**): $h/H = 0.48$. (**c**): $h/H = 0.74$.

4.2. Wave-Submerged Plate Interaction in the Presence of Current

After testing the validity of the proposed numerical approach, we will focus in this part on the effect of the current on the reflection coefficient. For this, Figure 5 depicts a comparison of our numerical results with the results of a corrected plane wave analytical model [17] and the experimental results of Rey and Touboul [12], by showing the variations of the reflection coefficient R as a function of the wave period T where the calculations were made in the presence of a current $U = 0.3$ m/s. According to the curves presented in this figure, we show that our numerical results better approach the experimental measurements compared to the analytical results, knowing that the numerical and analytical models do not take into account the generation of vortices by the plate.

The precision of the BEM result is good even if there is current, which justifies the choice of the BEM for this type of problem.

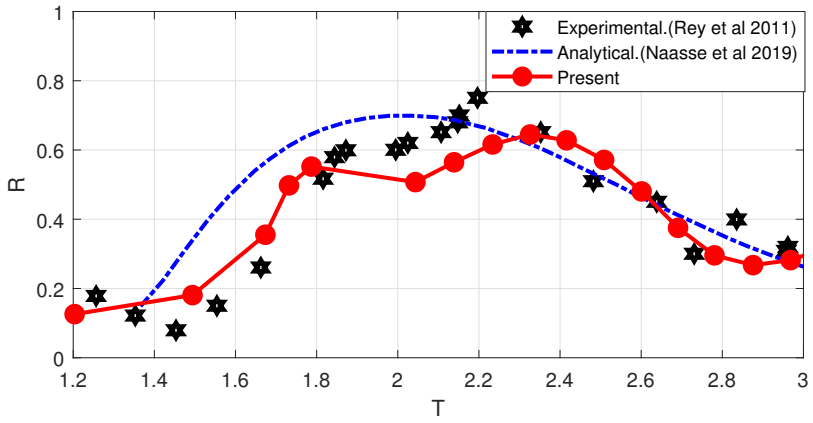

Figure 5. Comparison of the reflection coefficients of the present model with the analytical solution of Naasse et al. (2019) and the experimental data of Rey et al. (2011).

4.2.1. Effect of Geometric Parameters of the Plate

In the following, we consider a monochromatic incident wave of amplitude $a = 0.01$ m, propagating in a numerical wave tank (NWT) of length $L = 30$ m and depth $H = 2.5$ m, as well as a horizontal immersed plate of depth $h = 0.5H$, length $l = 1.5H$ and thickness $e = 0.1H$, with the presence of a current characterized by the Froude number $(F_r = U/\sqrt{gH}) = 0.04$.

First, we investigate the effect of plate thickness on the reflection coefficient and the free surface elevation. The obtained results in Figure 6 show that the reflection coefficient decreases as the thickness of the plate increases, which proves that the reflection coefficient of a thin plate is more effective than a thick plate.

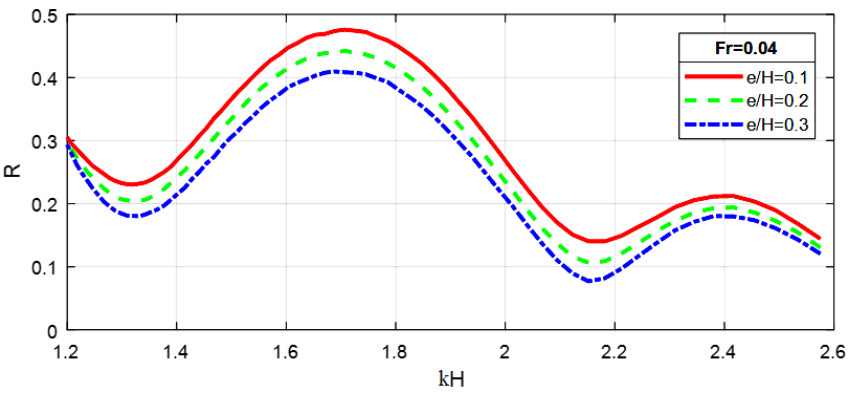

(**a**)

Figure 6. *Cont.*

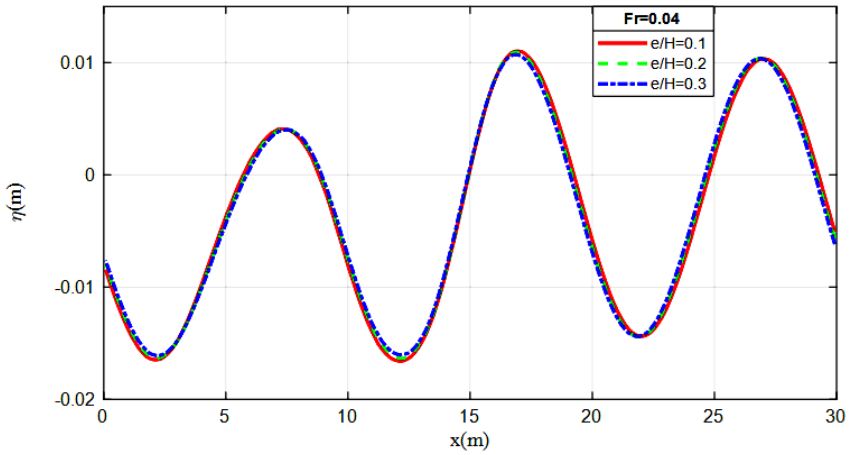

(**b**)

Figure 6. The effect of plate thickness on (**a**): the reflection coefficients and (**b**): the free surface elevation for $t = T$ and $\lambda = 9$ m.

Next, we discuss the effect of the length of the plate on the reflection coefficient and the free surface elevation. As illustrated in Figure 7, the reflection coefficient increases with the increase in the length of the plate, but the width of the reflection band decreases. Thus, the maximum of the reflection coefficient is shifted to the low wavenumber k. In addition, the deformation of the free surface elevation upstream of the plate increases with the plate thickness increase.

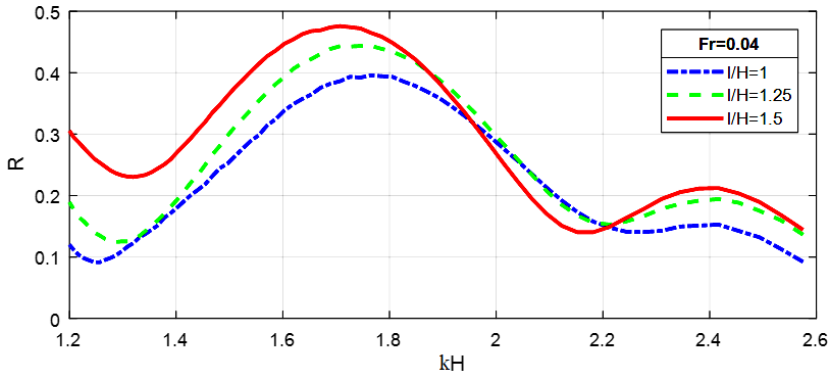

(**a**)

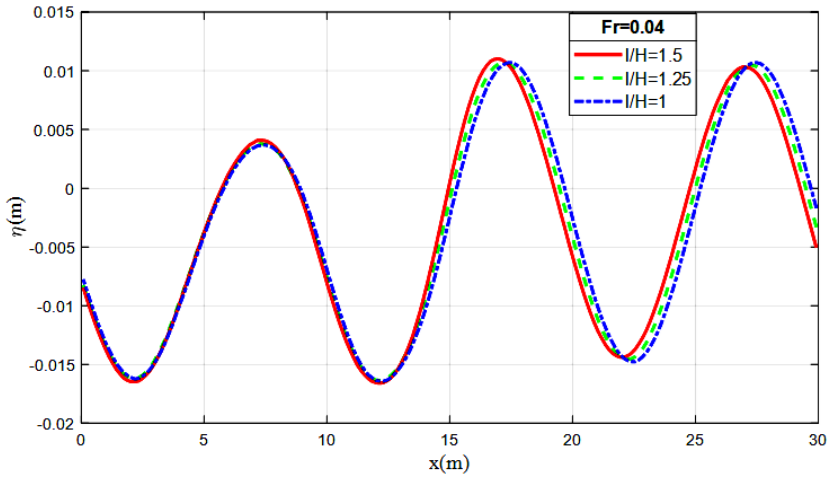

(**b**)

Figure 7. The effect of the plate length on (**a**): the reflection coefficients and (**b**): the free surface elevation for $t = T$ and $\lambda = 9$ m.

For the third investigation, we are interested in the effect of the immersion of the plate. According to Figure 8, we see that the coefficient of reflection and the deformation of the free surface elevation upstream of the plate decrease when immersion increases. This is explained by the fact that when the plate is more immersed, the amplitude of reflected water will attenuate because of the distance between the free surface and the plate.

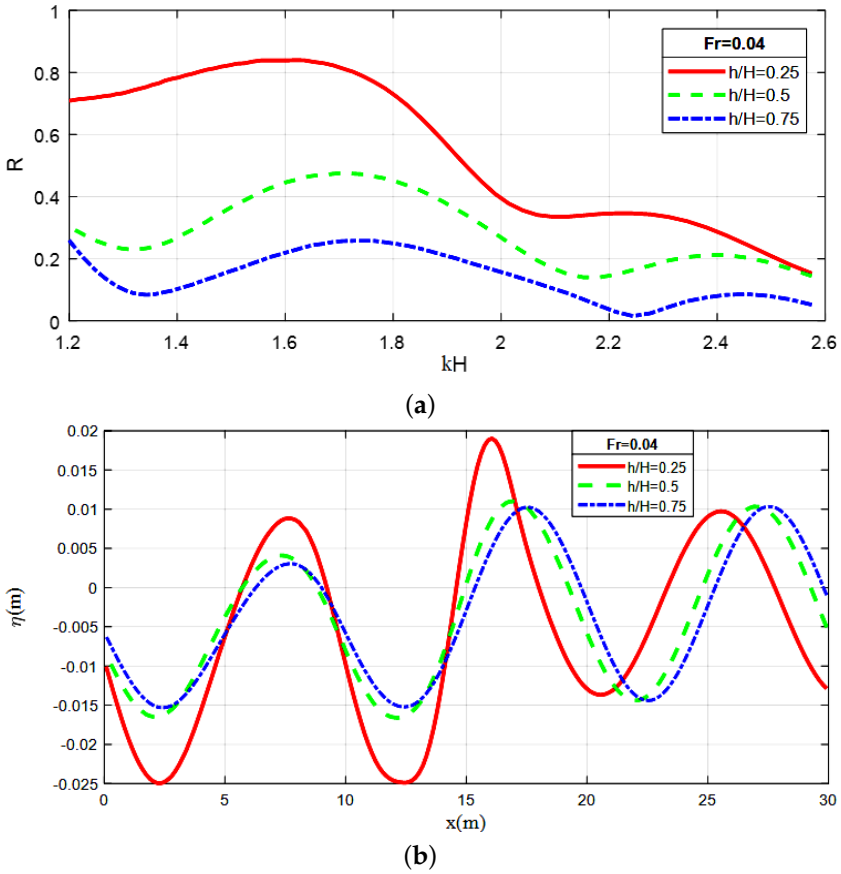

Figure 8. The effect of plate immersion on (**a**): the reflection coefficients and (**b**): the free surface elevation for $t = T$ and $\lambda = 9$ m.

4.2.2. Effect of the Current

Finally, we will study the influence of the current on the reflection coefficient and the free surface elevation. As shown in Figure 9 concerning the coefficient of reflection, the maximum of the latter and the width of the reflection band increase with the increase in the Froude number.

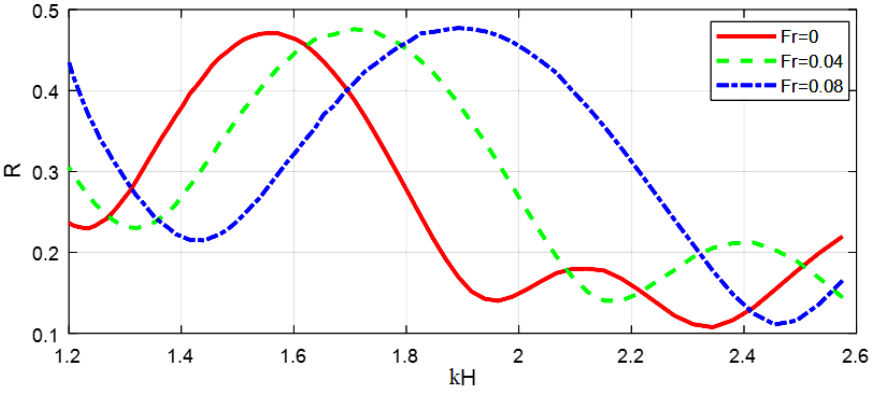

Figure 9. Reflection coefficient R as a function of kH for different values of the Froude number ($F_r = 0, 0.04, 0.08$).

Figure 10 shows the free surface elevation as a function of the length of the tank. According to Figure 10a–c, we can see a creation of nodes and bellies upstream of the plate. An increase in the width of the bellies is observed by increasing the current velocity, which is obvious because the increase in the current velocity implies the amplification of the wave and then an important reflection, as discussed previously. In the same sense, Figure 10d shows an increase in amplitude as well as a shift of the maximum and minimum downwards in the presence of the current and a phase shift linked to the amplification of the wave by the current.

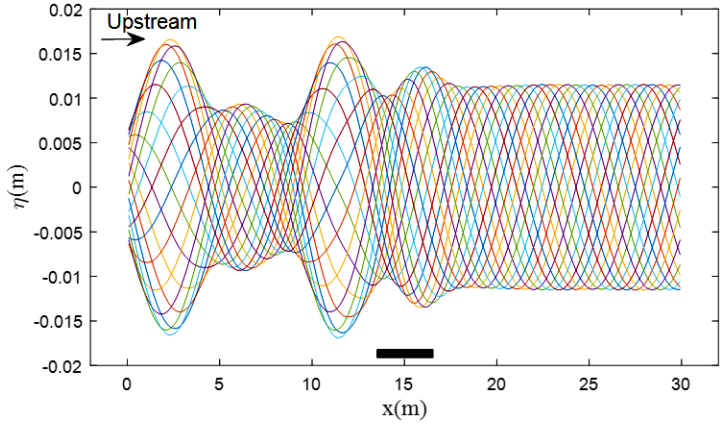

(**a**)

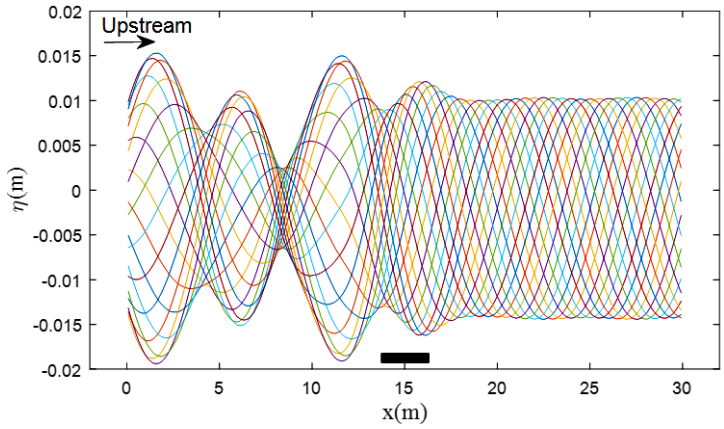

(**b**)

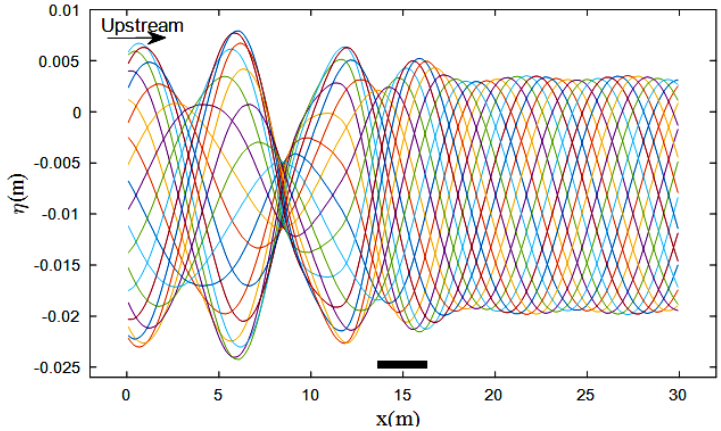

(**c**)

Figure 10. *Cont.*

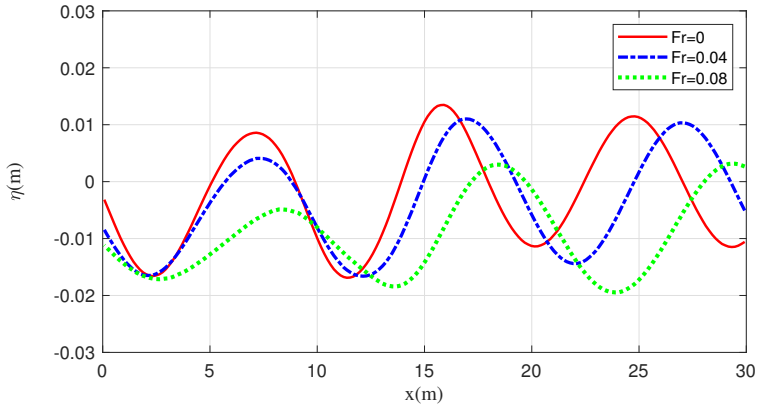

(**d**)

Figure 10. Elevation of the free surface as a function of channel length. (**a**): For different instants and $Fr = 0$. (**b**): For different instants. (**c**): For different instants and $Fr = 0.08$. (**d**): For $t = T$ at different Froude numbers.

5. Conclusions

In this work, we have numerically studied the problem of wave-plate interaction in the presence of a uniform current of the same direction as the incident wave propagation. The approach adopted consists of numerical modeling based on the boundary element method (BEM). This numerical approach is validated both in the absence and presence of the current by a comparison of the numerical linear solution with experimental results from the literature. Indeed, the numerical calculation code developed proves to be effective in calculating, on the one hand, the reflection coefficient and, on the other hand, the free surface elevation. We noticed that the geometry of the plate has a very important influence on the variation of the reflection coefficient as well as the free surface elevation. These results are used to better understand the mechanisms of wave attenuation and dissipation in the presence of current. This will help us to optimize the conception of the attenuators at the docks and ports and also predict the response of the wave.

Author Contributions: Conceptualization, H.A., L.E.A., L.M. and S.M.; methodology, H.A., L.E.A., L.M. and S.M.; software, H.A., L.E.A., L.M. and S.M.; validation, H.A., L.E.A., L.M. and S.M.; investigation, H.A., L.E.A., L.M. and S.M.; writing—original draft preparation, H.A., L.E.A., L.M. and S.M.; writing—review and editing, H.A., L.E.A., L.M. and S.M.; visualization, H.A., L.E.A., L.M. and S.M.; supervision, H.A., L.E.A., L.M. and S.M. All authors have read and agreed to the published version of the manuscript.

Funding: This research received no external funding.

Institutional Review Board Statement: Not applicable.

Informed Consent Statement: Not applicable.

Data Availability Statement: Not applicable.

Conflicts of Interest: The authors declare no conflict of interest.

Abbreviations

The following abbreviations are used in this manuscript:

BEM	boundary element method
NWT	numerical wave tank

References

1. Brossard, J.; Chagdali, M. Experimental investigation of the harmonic generation by waves over a submerged plate. *Coast. Eng.* **2001**, *42*, 277–290. [CrossRef]
2. Brossard, J.; Perret, G.; Blonce, L.; Diedhiou, A. Higher harmonics induced by a submerged horizontal plate and a submerged rectangular step in a wave flume. *Coast. Eng.* **2009**, *56*, 11–22. [CrossRef]
3. Liu, C.; Huang, Z.; Tan, S. Nonlinear scattering of non-breaking waves by a submerged horizontal plate: Experiments and simulations. *Ocean Eng.* **2009**, *36*, 1332–1345. [CrossRef]
4. Xie, Z.; Stoesser, T.; Yan, S.; Ma, Q.; Lin, P. A Cartesian cut-cell based multiphase flow model for large-eddy simulation of three-dimensional wave-structure interaction. *Comput. Fluids* **2020**, *213*, 104747. [CrossRef]
5. El Aarabi, L.; Mouakkir, L.; Mordane, S. Numerical Modeling of the Wave-Structure Interaction Using the Boundary Element Method. *Softw. Eng. Perspect. Intell. Syst.* **2020**, *1294* , 292–303.
6. Zou, Z.L.; Hu, P.C.; Fang, K.; Liu, Z. Boussinesq-type equations for wave-current interaction. *Wave Motion* **2013**, *50*, 655–675. [CrossRef]
7. Ning, D.; Lin, H.; Teng, B.; Zou, Q. Higher harmonics induced by waves propagating over a submerged obstacle in the presence of uniform current. *China Ocean Eng.* **2014**, *28*, 725–738. [CrossRef]
8. Ning, D.; Lin, H.; Teng, B.; Zou, Q. Study of interaction between wave-current and the horizontal cylinder located near the free surface. *Appl. Ocean. Res.* **2017**, *67*, 44–58.
9. Lim, K.Y.; Madsen, O.S. An experimental study on near-orthogonal wave–current interaction over smooth and uniform fixed roughness beds. *Coast. Eng.* **2016**, *116*, 258–274. [CrossRef]
10. Fan, C.M.; Chu, C.-N.; Sarler, B.; Li, T.H. Numerical solutions of waves-current interactions by generalized finite difference method. *Eng. Anal. Bound. Elem.* **2018**, *100*, 150–163. [CrossRef]
11. Hsiao, Y.; Tsai, C.-L.; Chen, Y.-L.; Wu, H.-L.; Hsiao, S.-C. Simulation of wave-current interaction with a sinusoidal bottom using OpenFOAM. *Appl. Ocean. Res.* **2020**, *94*, 101998. [CrossRef]
12. Rey, V.; Capobianco, R.; Dulou, C. Wave scattering by a submerged plate in presence of a steady uniform current. *Coast. Eng.* **2002**, *47*, 27–34. [CrossRef]
13. Rey, V.; Touboul, J. Forces and moment on a horizontal plate due to regular and irregular waves in the presence of current. *Appl. Ocean. Res.* **2011**, *33*, 88–99. [CrossRef]
14. Zhang, J.; Zhu, B.; Kang, A.; Yin, R.; Li, X.; Huang, B. Experimental and numerical investigation of wave-current forces on coastal bridge superstructures with box girders. *Adv. Struct. Eng.* **2020**, *23*, 1438–1453. [CrossRef]
15. Ning, D.; Chen, L.; Lin, H.; Zou, Q.; Teng, B. Interaction mechanisms among waves, currents and a submerged plate. *Appl. Ocean. Res.* **2019**, *91*, 101911. [CrossRef]
16. Errifaiy, M.; Naasse, S.; Chahine, C. Analytical determination of the reflection coefficient by the evanescent modes model during the wave-current-horizontal plate interaction. *Comptes Rendus Mécanique* **2016**, *344*, 479–486. [CrossRef]
17. Naasse, S.; Errifaiy, M.; Chahine, C. Analytical study of the effect of the geometrical parameters during the interaction of regular wave-horizontal plate-current. *Acta Oceanol. Sin.* **2019**, *38*, 10–20. [CrossRef]
18. Wrobel, L.C. *The Boundary Element Method, Volume 1: Applications in Thermo-Fluids and Acoustics*; John Wiley & Sons: Hoboken, NJ, USA, 2002.
19. Lee, J.-J. Wave-induced oscillations in harbours of arbitrary geometry. *J. Fluid Mech.* **1971**, *45*, 375–394. [CrossRef]
20. Dabsi, N. *Modélisation Numérique des Oscillations Induites Dans un Port Sollicité par une Houle Incidente et Étude du Comportement d'un Navire Amarré*; Université Hassan II, Faculté des Sciences Ben M'Sik: Casablanca, Morocco, 1998.
21. Airy, G.B. *Tides and Waves*; B. Fellowes: London, UK, 1845.